Available online at www.sciencedirect.com

SCIENCE DIRECT®

Earth and Planetary Science Letters 222 (2004) 845–862

EPSL

www.elsevier.com/locate/epsl

Three-dimensional distribution of gas hydrate beneath southern Hydrate Ridge: constraints from ODP Leg 204

A.M. Tréhu[a,*], P.E. Long[b], M.E. Torres[a], G. Bohrmann[c], F.R. Rack[d], T.S. Collett[e], D.S. Goldberg[f], A.V. Milkov[g,1], M. Riedel[h], P. Schultheiss[i], N.L. Bangs[j], S.R. Barr[k], W.S. Borowski[l], G.E. Claypool[m], M.E. Delwiche[n], G.R. Dickens[o], E. Gracia[p], G. Guerin[f], M. Holland[q], J.E. Johnson[a], Y.-J. Lee[r], C.-S. Liu[s], X. Su[t], B. Teichert[u], H. Tomaru[v], M. Vanneste[w], M. Watanabe[x], J.L. Weinberger[y]

[a] *College of Oceanic and Atmospheric Science, Oregon State University, Corvallis, OR 97331-5503, USA*
[b] *Pacific Northwest National Laboratory, Richland, WA 99352, USA*
[c] *Department of Geosciences, University of Bremen, Klagenfurterstr. D-28359 Bremen, Germany*
[d] *JOI, 1755 Massachusetts Ave. NW, suite 700, Washington, DC 20036, USA*
[e] *U.S. Geological Survey, Denver Federal Center, Denver, CO 80225, USA*
[f] *Borehole Research Group, Lamont-Doherty Earth Observatory, Palisades, NY 10964, USA*
[g] *Geology and Geophysics, WHOI, Woods Hole, MA 02543, USA*
[h] *Geological Survey of Canada, Pacific Geoscience Centre, Sidney BS, Canada V8L4B2*
[i] *GEOTEK, Daventry, Northants, NN11 5RD, UK*
[j] *Institute for Geophysics, University of Texas at Austin, 4412 Spicewood Springs Rd., Austin, TX 78759, USA*
[k] *Department of Geology, University of Leicester, Leicester, LE1 7RH, UK*
[l] *Department of Earth Sciences, Eastern Kentucky University, 512 Lancaster Ave., Richmond, KY 40475, USA*
[m] *8910 West 2nd Avenue, Lakewood, CO 80226, USA*
[n] *Idaho National Engineering and Environmental Laboratory, Idaho Falls, ID 83415-2203, USA*
[o] *Department of Earth Science, Rice University, Houston, TX 77005, USA*
[p] *Unitat de Tecnologia Marina, Centre Mediterrani d'Investigacions Marines i Ambientals, 08003 Barcelona, Spain*
[q] *Department of Geological Sciences, Arizona State University, Tempe, AZ 85287, USA*
[r] *Petroleum and Marine Resources Research Division, Korea Institute of Geoscience and Mineral Resources, Daejon 305-350, South Korea*
[s] *Institute of Oceanography, National Taiwan University, Taipei 106, Taiwan*
[t] *Center of Marine Geology, China University of Geosciences, Beijing, People's Republic of China*
[u] *Forschungszentrum Ozeanrander, Universitat Bremen, Fostfack 330440, D-28334 Bremen, Germany*
[v] *Department of Earth and Planetary Science, University of Tokyo, Tokyo 113-0033, Japan*
[w] *Department of Geology, University of Tromso, 9037 Tromso, Norway*
[x] *Geoscience Institute, Geological Survey of Japan, Tsukuba 305-8567, Japan*
[y] *Scripps Institution of Oceanography, University of California, San Diego, CA 92093-0244, USA*

Received 21 August 2003; received in revised form 2 February 2004; accepted 23 March 2004

* Corresponding author.
E-mail address: trehu@coas.oregonstate.edu (A.M. Tréhu).
[1] Present address: BP America, Houston, TX 77079, USA.

0012-821X/$ - see front matter. Published by Elsevier B.V.
doi:10.1016/j.epsl.2004.03.035

Abstract

Large uncertainties about the energy resource potential and role in global climate change of gas hydrates result from uncertainty about how much hydrate is contained in marine sediments. During Leg 204 of the Ocean Drilling Program (ODP) to the accretionary complex of the Cascadia subduction zone, we sampled the gas hydrate stability zone (GHSZ) from the seafloor to its base in contrasting geological settings defined by a 3D seismic survey. By integrating results from different methods, including several new techniques developed for Leg 204, we overcome the problem of spatial under-sampling inherent in robust methods traditionally used for estimating the hydrate content of cores and obtain a high-resolution, quantitative estimate of the total amount and spatial variability of gas hydrate in this structural system. We conclude that high gas hydrate content (30–40% of pore space or 20–26% of total volume) is restricted to the upper tens of meters below the seafloor near the summit of the structure, where vigorous fluid venting occurs. Elsewhere, the average gas hydrate content of the sediments in the gas hydrate stability zone is generally <2% of the pore space, although this estimate may increase by a factor of 2 when patchy zones of locally higher gas hydrate content are included in the calculation. These patchy zones are structurally and stratigraphically controlled, contain up to 20% hydrate in the pore space when averaged over zones ~10 m thick, and may occur in up to ~20% of the region imaged by 3D seismic data. This heterogeneous gas hydrate distribution is an important constraint on models of gas hydrate formation in marine sediments and the response of the sediments to tectonic and environmental change.
Published by Elsevier B.V.

Keywords: gas hydrates; Ocean Drilling Program; methane; accretionary margins; marine sediments

1. Introduction

Gas hydrates are ice-like compounds that form at the low temperature and high pressure conditions common in marine sediments at water depths greater than 300–500 m when concentrations of methane and other low molecular weight gases exceed saturation. Although estimates of the total mass of methane carbon that resides in this reservoir vary widely e.g. [1,2] even conservative estimates are large, and it is likely that gas hydrates are a significant component of the global near-surface carbon budget [3]. Considerable controversy remains, however, about whether gas hydrates represent a major future fossil fuel resource e.g. [4,5] and whether they can contribute to global environmental change through destabilization and massive release of methane from the seafloor e.g. [6–8].

At the root of the controversy are large uncertainties about how gas hydrates and free gas are distributed within marine sediments. Gas hydrates decompose rapidly when removed from the high-pressure, deep-water environments in which they form, and much of the gas hosted in these compounds or present as free gas in the sediment pore space is lost during sample recovery. Moreover, even for cores recovered in an autoclave at in situ pressure, which retain all the gas present at depth, the gas released may be derived from gas hydrate dissociation, free gas bubbles, or exsolution of dissolved gas from pore water. The in situ distribution of gas hydrate must therefore be estimated using various proxy techniques, each of which may have different sensitivity and spatial resolution.

For the past several decades, the main proxy used to evaluate the regional presence of gas hydrate in seafloor sediments has been a seismic reflection known as the bottom simulating reflection (BSR). The BSR mimics the seafloor at approximately the sub-seafloor depth predicted to be the base of the gas hydrate stability zone (GHSZ) and has a negative polarity, indicating that it results from relatively high-velocity sediments containing gas hydrate that overlie low-velocity sediments containing free gas. Methods to estimate the gas hydrate content of continental margin sediments using seismic data have recently been reviewed [9].

Additional proxies (see Section 3) are available when sediments are drilled, logged and sampled. Data to validate estimates based on seismic data, however, are limited because the BSR has been drilled at only a handful of sites worldwide. Legs 141 and 146 of the Ocean Drilling Program (ODP), to the Chile triple junction region and Cascadia subduction zone, respectively, provided valuable insights into fluid flow, tectonics and hydrate formation in accretionary complexes [10,11], but quantitative determination of the

amount of gas hydrate present was limited by the lack of any samples recovered at in situ pressure. ODP Leg 164 on Blake Ridge offshore the southern U.S. was the only ODP leg prior to Leg 204 that was dedicated to understanding marine gas hydrates [12]. The three sites sampled during this leg were located in similar structural and stratigraphic settings. Little variation in gas hydrate distribution was observed between sites, and it is difficult to extrapolate from the results to other settings.

In this paper, we integrate results from a variety of methods with different spatial resolution and sensitivity in order to estimate the in situ gas hydrate content of sediments beneath southern Hydrate Ridge, which is part of the accretionary complex of the Cascadia subduction zone. All nine sites drilled during ODP Leg 204 are located within a volume imaged by three-dimensional seismic data and represent a wide range of structural and stratigraphic settings. We use robust techniques for estimating the gas hydrate content of core samples to calibrate estimates derived from geophysical techniques, which require additional assumptions to derive quantitative estimates of gas hydrate content but provide better spatial sampling. We thus obtain a quantitative improvement in our knowledge of how much gas hydrate is present in accretionary complex sediments and how it is distributed.

2. Geologic setting

During ODP Leg 204, nine sites were drilled and cored on southern Hydrate Ridge, a peanut-shaped topographic high in the accretionary complex of the Cascadia subduction zone, located approximately 80

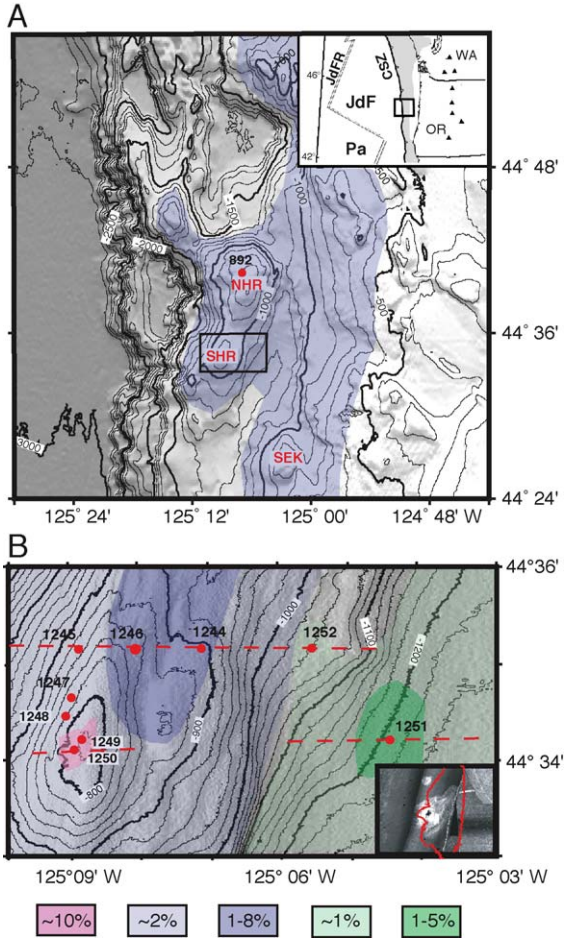

Fig. 1. (A) Bathymetric map of the accretionary complex offshore Oregon. Contour interval is 100 m. Red dot shows the location of ODP Site 892, drilled during Leg 146. Box shows the location of (B). Transparent violet overlay shows where a BSR is present in seismic data. Inset shows the tectonic setting of (A). Cascade volcanoes are shown as triangles. SHR—South Hydrate Ridge; NHR—North Hydrate Ridge; SEK—Southeast Knoll; OR—Oregon; WA—Washington; JdF—Juan de Fuca plate; Pa—Pacific plate; JdFR—Juan de Fuca ridge; CSZ—Cascadia subduction zone. (B) High-resolution (15m pixel) bathymetric map [42] of the region studied during ODP Leg 204. Contour interval is 20 m. Red dots show the location of sites drilled during Leg 204. Several holes were drilled at each site. Dashed red lines show locations of vertical slices through the 3D seismic data shown in Fig. 2. Transparent color overlays show the lateral extent of zones of different gas hydrate content, estimating by averaging the data from the seafloor to the BSR (Tables 1 and 2). The dark violet and dark green patterns outline regions in the data suggest that gas hydrate occurs in patchy zones of locally higher concentration, leading to high variability among estimates of gas hydrate content in boreholes spaced tens of meters apart. The inset shows the seafloor acoustic backscatter pattern at the summit of southern Hydrate Ridge [17] with light colors indicating high backscatter. The 800 m depth contour is shown for reference. The dark spot in the center of the region of high backscatter is the shadow of a carbonate pinnacle. Observations made with the DSV *Alvin* indicate that the very strong seafloor reflectivity around the pinnacle results from carbonate pavement (possibly mixed with gas hydrate) whereas the mottled reflective pattern results from gas hydrate at or near the seafloor. A larger version of this image, and its correlation with the seismic data, is found in [20].

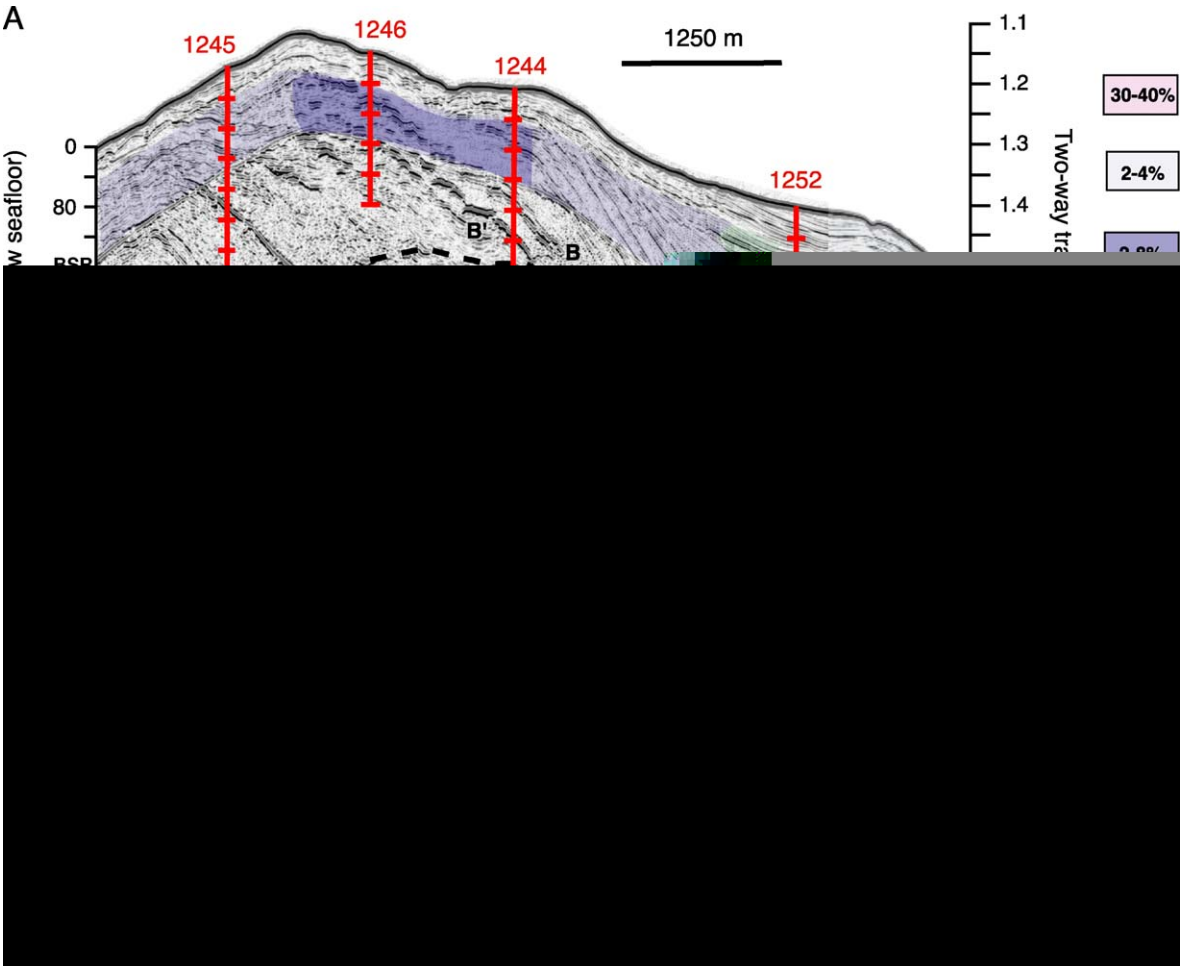

Fig. 2. Profiles extracted from the 3D seismic data along the lines shown in Fig. 1B. Black—strong positive amplitude; gray—positive amplitude; white—strong negative amplitude. Transparent overlays indicate zones of different average gas hydrate concentration estimated as discussed in the text. Although overlay colors are the same as in Fig. 1B, values of gas hydrate content in these zones are larger than in Fig. 1B, because here the values represent averages over the gas hydrate occurrence zone rather than over the gas hydrate stability zone. Vertical red bars show sites drilled during Leg 204; tick marks are spaced 75 m apart. AC—top of the highly deformed sediments of the accretionary complex; B—seismic horizon B, which was found to be coarse-grained and gas hydrate-rich at Site 1246; A—seismic horizon A, interpreted as a stratigraphically controlled zone along which methane-rich fluids migrate from the accretionary complex to the southern summit [14,15].

km west of Newport, OR (Fig. 1). Sites were chosen to complement ODP Site 892, drilled near the summit of northern Hydrate Ridge during ODP Leg 146. Site 892, which was drilled where the BSR is anomalously shallow as a result of fluid flow along a structure interpreted to be a fault [11], provided samples of H_2S-rich hydrates near the seafloor [11,13], "soupy" layers with anomalously low pore water Cl^- concentration, indicative of dissociation of gas hydrate on recovery [11,13], geochemical indications of migration of thermogenic methane into the GHSZ from greater depth [13,14], and the presence of a small amount of free gas beneath the GHSZ [15].

Although seafloor evidence for venting is less pervasive at southern Hydrate Ridge, compared to northern Hydrate Ridge [16,17], previous seafloor studies of southern Hydrate Ridge had documented the presence of seafloor gas vents, outcrops of mas-

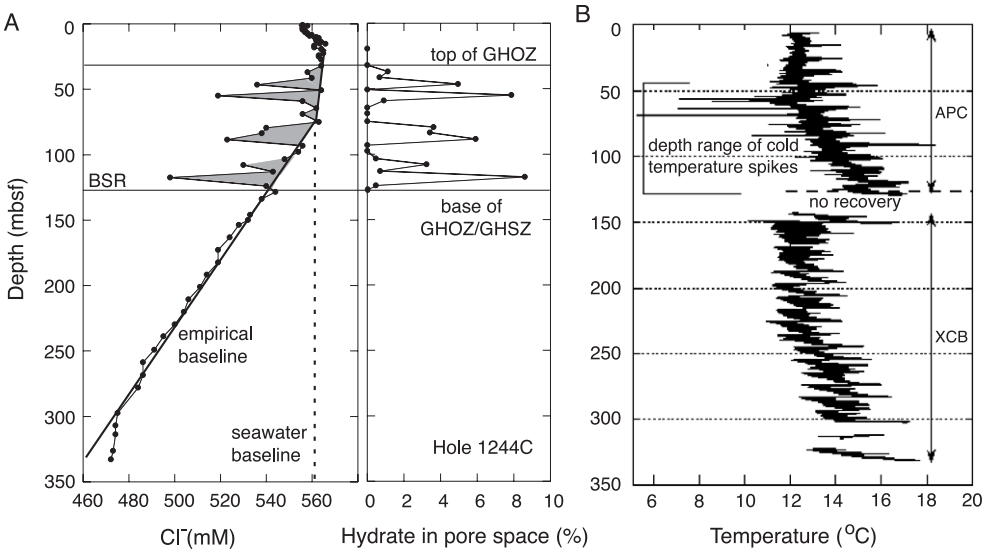

Fig. 4. (A) Cl^- concentration measured in Hole 1244C. The empirical baseline used for this study and a seawater baseline are shown. The gas hydrate content of the sediments determined assuming the empirical baseline is also shown. Uncertainties due to uncertainties in the empirical baseline are discussed in the Leg 204 Initial Report [20]. The seawater baseline would lead to a thick zone of significantly higher gas hydrate concentration in the lower portion of the GHSZ. We prefer the empirical baseline because chemical characteristics of the observed Cl^- concentration suggest a source of fresh water at depth [20]. (B) Temperature of cores recovered from Hole 1244C measured by scanning cores on the catwalk with an IR thermal camera. Temperature profiles were extracted from the thermal images by averaging across the central portion of the image. Cold "spikes" attributed to gas hydrate dissociation stand out from this complicated temperature structure, which depends on may factors, including the geothermal gradient, the position within a core, the ambient temperature on the catwalk, and the type of coring tool used. We note that cores obtained with the extended core barrel (XCB) cores are significantly cooler than cores obtained with the advanced piston corer (APC), probably due to the cooling effect of drilling fluid.

mechanisms to explain pore water dilution below the BSR e.g. [27].

One surprising result of Leg 204 was recovery of pore waters with Cl^- concentration much higher than seawater near the summit [20,28,29]. Where this is observed (in the upper 20–40 mbsf at Sites 1249 and 1250), no estimates of gas hydrate content were attempted because the baseline could not be defined. Implications of these interstitial brines for models of gas hydrate dynamics will be discussed elsewhere [28].

Because of physical limitations on how much pore water can be extracted and the time needed for each measurement, this technique provides relatively sparse measurements. During Leg 204, two measurements were generally made in each core from within the gas hydrate stability zone (GHSZ), for a downhole measurement interval of ~5 m. Each sample represents 5–10 cm of core squeezed and analyzed according to standard ODP procedures.

3.3. Infrared thermal scans of cores

Because hydrate dissociation is an endothermic reaction, intervals in sediment cores where gas hydrate is dissociating, or has recently dissociated, are relatively cold [30]. These cold spots can be felt by hand [12] or measured with infrared (IR) thermal cameras [30]. Leg 204 is the first ODP leg during which all cores from within or near the predicted gas hydrate stability zone were systematically scanned with a track-mounted digital IR thermal camera as soon as possible after recovery. Fig. 3B shows close-up views of two typical IR cold anomalies and the gas hydrate lens and nodules exposed when the cores were split. Although it is possible that some IR cold temperature anomalies result from other effects, such as decompression of gas pockets, numerous examples similar to those shown in Fig. 3B are documented in the Leg 204 Initial Report [20] and suggest that distinct, strong cold anomalies are a reliable indicator

of hydrate presence. In fact, gas expansion pockets generally seem to have equilibrated with the ambient temperature and appear as warm spots [20].

The right side of Fig. 3A shows IR temperature anomalies from a 6-m length of core at Site 1244. The dark horizontal lines are IR cold anomalies. Most anomalies are only a few centimeters long and their distribution is highly variable. The spacing of gas hydrate layers indicated in the HYACINTH pressure core (~0.65 m) is similar to the spacing of IR anomalies in the overlying core. Although no strong temperature anomalies indicative of lenses of gas hydrate are detected in the 2 m of core recovered from immediately beneath the pressure core, another pair of closely spaced cold anomalies occurred at 58–59 mbsf, indicating the strong heterogeneity of gas hydrate distribution. This figure also shows the typical length and spacing of samples taken for pore water analysis. The minimum practical sampling interval for both the PCS (~3/hole) and the pore water (~5 m) data and the length over which each sample is averaged are clearly too large to characterize the vertical variation in gas hydrate distribution.

Temperature profiles of cores measured by the IR camera depend on many different variables. Fig. 4B shows the temperature profile averaged across the central portion of each IR image for Hole 1244C. Large amplitude (>2 °C) cold spikes stand out relative to the local background temperature and are only found within the gas hydrate stability zone (GHSZ). A detailed view of one such anomaly is shown in Fig. 5A. The anomaly can be characterized by its amplitude (ΔT) and length (ΔL) relative to the local background temperature trend. To calibrate the IR data, we sampled pore waters at intervals of ~2 cm in the section of core for which the anomaly shown in Fig. 5A had been observed (Fig. 5B). The depth extent of the Cl^- concentration anomaly is similar to the depth extent of the IR anomaly, and differences in depth between the two anomalies result from compression of the core to close gas voids after the core was scanned and before samples were taken for Cl^- analysis. The hydrate content derived by integrating over the Cl^- concentration anomaly is 40% of sediment pore space. These data were used to define an empirical relationship between the hydrate content of a borehole and the amplitude (ΔT) and depth range (ΔL) of IR anomalies. Uncertainties in this relationship are discussed in Section 4.

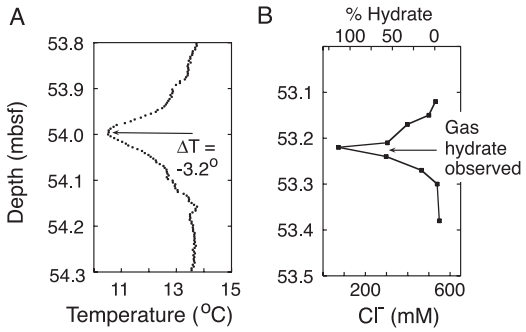

Fig. 5. (A) The temperature profile derived from an IR image that showed a cold spot (from Core 1245C-7H-5). ΔT and ΔL are indicated. (B) Chloride concentrations in closely spaced pore water samples along the core corresponding to the temperature profile in (A). The apparent offset in depth between the two graphs is due to compression of the core to close gas expansion voids between the time when the IR image was made and the pore water samples were taken. This can result in offsets of as much as 1 m between depths recorded on the track-mounted IR temperature scans and depths logged for core samples.

3.4. Resistivity-at-bit (RAB)

The electrical resistivity of gas hydrate is higher than that of saturated sediments. RAB images represent the electrical resistivity as a function of azimuth around the borehole measured at the drill bit as a hole is drilled. Leg 204 was the first ODP leg during which Logging-While-Drilling (LWD) data were acquired at sites that had never been cored [20]. The presence of gas hydrate within the GHSZ is apparent in borehole resistivity images [20]. The percentage of gas hydrate in the pore space can be estimated by estimating the percentage of pore space filled by water using the Archie's relation and by assuming that gas hydrate fills the rest of the pore space [31,32]. During Leg 204, the RAB data, in conjunction with the 3D seismic data discussed above, provided a ''road map'' that guided subsequent coring, permitting us to anticipate when we would be sampling zones rich in gas hydrate.

This technique provides a continuous record of the subsurface with a spatial resolution in the vertical and horizontal directions of a few centimeters as long as drilling conditions are good, as monitored by caliper measurements [20]. It does not, however, distinguish

between gas hydrate and free gas in the pore space because both gas hydrate and free gas are characterized by low electrical resistivity. If free gas coexists with gas hydrate, the gas hydrate concentration will be overestimated. There may also be other uncertainties associated with use of the empirically derived Archie relationship, making it desirable to compare RAB-based estimates of gas hydrate content with estimates derived from other measurements.

3.5. Other geophysical logs

Several other geophysical logging techniques that can constrain the gas hydrate content of the subsurface were employed during Leg 204, including nuclear magnetic resonance (NMR), sonic logs and vertical seismic profiling [20]. These techniques provide a continuous record of the physical properties of sediments within the borehole with a spatial resolution that varies from centimeters for wire line sonic logs e.g. [33] to meters for vertical seismic profiles (VSP) e.g. [15]. In addition, offset and walkaway VSPs provide a means of extending borehole results into the region around the borehole [34]. Estimates of the gas hydrate or free gas content of the sediments from these geophysical logs, however, depend strongly on assumptions about how the gas hydrate is distributed within the sediments [9]. The results summarized in this paper will be useful for testing and calibrating the results of ongoing studies of other geophysical logs from Leg 204 and elsewhere.

4. Estimating the average gas hydrate content of cores from IR data

In this section, we discuss our procedure for calculating the average gas hydrate content of a drill hole from IR temperature anomalies. Results are compiled in Table 1 and compared to averages based on PCS, Cl^- concentration and RAB data. Average gas hydrate contents are cited as a percentage of the pore space filled by gas hydrate because this is the natural unit for estimates based on Cl^- anomalies. We do not, however, mean to imply that all of the gas hydrate present beneath Hydrate Ridge is disseminated in the pore space. Leg 204 observations clearly indicate that hydrate is present in lenses and nodules that have displaced sediment [20], and hydrate in this form is more appropriately expressed in terms of percentage of total volume. Conversion between these two conceptual frameworks is simple because the average porosity of sediments within the gas hydrate stability zone is ~65% at all sites [20].

The average gas hydrate content of cores was calculated from IR data as follows. The amplitude (ΔT) and length (ΔL) of each IR anomaly relative to the local background temperature was picked from the temperature profile derived from IR images of that core. Tabulated ΔT and ΔL picks as well as many examples of IR scans can be found in the Site chapters of the Leg 204 Initial Report [15]. The number of IR anomalies and the average ΔT and ΔL in each hole are given in Table 1 to show general patterns.

Based on the calibration experiment shown in Fig. 5, ΔT anomalies of amplitude 0–1, 1–3 and >3 °C, respectively, were defined to represent hydrate contents of 10%, 30%, and 50% of pore space. We refer to this calibration function as the "threshold" function. The sensitivity of estimates over average gas hydrate content based on the threshold function were evaluated by comparing the results to those obtained using a linear function passing through 40% for ΔT=−3.2 °C. The linear function is particularly sensitive to a few large anomalies, which have amplitudes as great as 7 °C, and is less sensitive to the many small anomalies with amplitude <1 °C. The two methods agree to within 20% although the average gas hydrate content is slightly lower for most, but not all, of the holes when the linear function is used. Because the amplitude of an anomaly depends strongly on where the hydrate occurs relative to the core liner [20], we prefer the threshold function. Additional work to calibrate IR temperature anomalies, however, is needed.

The average hydrate content within gas hydrate stability zone (GHSZ) was calculated by summing the length of all anomalies in each category, converting this to hydrate content, and then averaging the hydrate content over the thickness of the GHSZ. The base of the GHSZ was determined from the BSR depth, which is in all cases within a few meters of the depth of the deepest observed IR anomaly [20]. The top of the GHSZ for this calculation was defined to be the seafloor, although the GHSZ extends several hundred meters into the water column [35]. Average concentrations were also determined within the gas hydrate occurrence zone

Table 1
Spacing and amplitude of IR temperature anomalies and hydrate content of sediments expressed as percent of pore space from IR and other data

ODP hole (1)	BSR depth (m)	Depth range of RAB or IR an. (m)	No. of IR an.	Mean ΔT (°C)	Mean ΔL (m)	% Recovery	Mean spacing GHOZ (2) (m)	% Hydrate from ΔT in GHOZ/ GHSZ (2,3)	% Hydrate from PCS in GHOZ/ GHSZ (4,7)	% Hydrate from Cl^- in GHOZ/ GHSZ (5,7)	% Hydrate from RAB GHOZ/ GHSZ (6,7)
Hydrate Ridge—away from summit											
1244B	124	–	–	–	–	–	–	–	–	–	8.1/6.1
1244C	124	45–125	31	−1.6	0.25	95	2.6	3.2/2.0	0/0	2.2/2	–
1244E	124	23–121	49	−1.8	0.18	101	2.0	2.6/2.1	0.9/1.4	3.5/1.8	–
1245A	134	–	–	–	–	–	–	–	–	–	3.1/1.9
1245B	134	52–119	35	−2.4	0.16	89	2.0	3.8/1.9	–	3.0/2.0	–
1245C	134	44–120	40	−1.6	0.16	93	1.6	2.9/1.6	4.0/6.0	–	–
1246A	114	–	–	–	–	–	–	–	–	–	1.5/1.0
1246B	114	16–117	53	−1.3	0.47	98	1.8	5.6/5.0	–	2.3/1.7	–
1247A	124	–	–	–	–	–	–	–	–	–	2.0/1.6
1247B	130	16–116	49	−1.1	0.19	98	2.0	1.9/1.5	1.3/2.6	1.5/0.8	–
Hydrate Ridge—summit											
1248A	115	–	–	–	–	–	–	–	–	–	17/7
1248C	115	1–124	57	−3.4	0.39	68	1.5	7.3	–	4.5	–
	115	1–30	7	−2.2	0.94	26	1.1	18.0	–	n.b.	–
1249A	115	–	–	–	–	–	–	–	–	–	73/75
1249F	115	1–88 (8)	48	−3.1	0.32	70	1.1	13.9	23	n.b.	–
	115	1–30	14	−4.2	0.47	39	0.9	23.6	43	n.b.	–
	115	30–88	34	−2.8	0.29	79	1.3	11.8	4.6	2.0	–
1250A	114	–	–	–	–	–	–	–	–	–	26/5
1250C	114	14–109	40	−1.6	0.19	82	1.8	2.6	0.7	4.3	–
	114	1–14	–	–	–	0	–	–	–	n.b.	–
1250D	114	7–114	57	−1.2	0.18	94	1.8	1.8	1.4	–	–
Slope basin											
1251A	200	–	–	–	–	–	–	–	–	–	1.2/1.0
1251B	200	41–188	13	−1.0	0.58	83	9.4	1.6/1.2	0.5/0.5	b.d.	–
1251D	200	34–205	14	−1.6	1.50	86	10.4	5.2/4.5	0.2/0.2	2.8/1.7	–
1252A	170	19–183	33	−0.8	0.27	98	4.9	1.9/1.3	–	b.d.	–

(1) Sites are designated by numbers; holes at a site are designated by letters.
(2) Corrected for % recovery.
(3) Average gas hydrate content from IR data was calculated as discussed in the text. Results are shown for integration over the gas hydrate occurrence zone (GHOZ), defined as the depth range over which indicators for gas hydrate were observed, and the gas hydrate stability zone (GHSZ), defined as the region from the seafloor to the BSR. At Site 1252, the projected depth of the BSR was used. For the summit region, the GHOZ and the GHSZ are the same because indicators of gas hydrate presence extend from the BSR to the seafloor. At these sites, the gas hydrate content of the shallow zone of massive hydrate is given separately.
(4) Each number represents the average of one to three samples spaced at unequal intervals. Each sample averages gas hydrate content over ~1 m. No PCS data were acquired in Holes 1245B, 124B, 1248C or 1252A. Measurement uncertainties are discussed elsewhere [2].
(5) These estimates represent averages of 15–30 samples/hole spaced at unequal intervals. Each sample averages gas hydrate content over 5–10 cm of core length. Uncertainties due to uncertainties in the baseline are estimated to be ±0.5%. b.d.: indicates that any hydrate present was below the detection level of this technique. n.b.: indicates that no baseline could be estimated because of anomalously high Cl^- concentration.
(6) Averages were calculated from pore water saturation estimates based on electrical resistivity data and tabulated at ~15-cm intervals and include hundreds of data points. These data require no correction for core recovery. No RAB data were acquired at Site 1252. Note that all RAB data are from the "A" hole at a given site, except from Site 1244, where they are from the "B" hole. Holes characterized by RAB data are ~50 m away from other holes at that site.
(7) All measurements in the GHOZ or GHSZ were included in the average, including data points indicating no gas hydrate.
(8) 88 mbsf is the depth at the bottom of this hole, which is ~24 m above the BSR.

(GHOZ), defined as the depth range over which IR anomalies were observed. As discussed below in Section 5, only near the summit were any significant gas hydrate indicators observed in the upper ~40 mbsf. Because core temperature is sampled at an interval corresponding to the resolution of the IR scan (~1 cm), the calculated % hydrate represents an integration over hundreds of samples representing all sediments recovered, even though a given core contains many fewer identified anomalies. This contrasts with averages based on PCS and Cl^- concentration data, which generally sample <3% of the sediment in a borehole.

The primary sources of uncertainty in the IR-based estimates of gas hydrate content are: (1) incomplete core recovery; (2) uncertainty in the function used to convert ΔT to hydrate content; (3) uncertainty about whether all picked anomalies are due to gas hydrate; and (4) uncertainty about whether all hydrate results in a recognized anomaly. Values given in Table 1 for gas hydrate concentration were corrected for incomplete recovery by dividing by the fraction of core recovered, which was generally >90% except near at the summit. This correction assumes that the hydrate content of sediments that were not recovered is the same as in the recovered sediments; this assumption probably underestimates the average gas hydrate content because, given the generally homogeneous nature of the sediments, high gas hydrate content was probably a major reason for poor core recovery during Leg 204 [20].

It is difficult to evaluate whether all picked anomalies represent in situ hydrate. Anomalies observed at Sites 1244–1247 at depths shallower than 40 mbsf, where no hydrate was detected in PCS or Cl^- concentration measurements, may result from gas expansion rather than from gas hydrate. If those anomalies are excluded from the integration, estimates integrated over the GHSZ decrease slightly; however, for Hole 1246B, the estimate increases for the GHOZ because the shallow anomalies are all of low amplitude and thus "dilute" the estimate for hydrate in the GHOZ. More problematic is the fact that our approach to picking IR anomalies may miss gas hydrate homogeneously disseminated over length scales of greater than a few centimeters; this would result in a broad anomaly that would not stand out sharply from other background temperature variations, leading to an underestimate in the average gas hydrate concentration obtained by this technique.

5. Small-scale heterogeneity in gas hydrate distribution

Vertical variation in gas hydrate content for several sites is shown in Fig. 6. We discuss the results at Site 1245 in detail to obtain some preliminary insights into the scale length of spatial variation in gas hydrate distribution. These preliminary observations will undoubtedly be refined through ongoing analysis of the data from Leg 204. At Site 1245, and at all other sites with the exception of those near the summit, no unambiguous indicators of gas hydrate were found in the upper ~40 m beneath the seafloor. All proxies indicate that gas hydrate is present sporadically between ~40 mbsf and the BSR at 134 mbsf. IR anomalies indicate that hydrate lenses or nodules a few centimeters thick have an average spacing of ~2 m in the GHOZ and are clustered between 56 and 60 mbsf, 80 and 100 mbsf, and just above the BSR at ~134 mbsf. A detailed look at the azimuthal distribution within one of these clusters obtained from the RAB data shows the three dimensional nature of heterogeneity in gas hydrate distribution on the centimeter scale (Fig. 4A).

Assuming that the average spacing between IR temperature anomalies of 2 m is an accurate indication of the in situ spacing of hydrate lenses away from the summit, we can use this distribution to predict how many PCS or Cl^- concentration measurements should indicate the presence of hydrate and thus evaluate potential spatial biases in these measurements. Half of the PCS cores, which are nominally 1 m long, should capture a hydrate lens. Although the total number of PCS samples is too small to be statistically significant, this is indeed what was observed. Methane levels above saturation were obtained in one out of two cores from the GHOZ at Site 1245 and in three out of six cores in the combined data set for Sites 1244–1247 if we include a PCS core from 39.5 mbsf. However, the concentration estimated by averaging estimates based on PCS data is not very robust and depends strongly on a single data point that indicates a gas hydrate content of 12% at a depth of 121 mbsf in Hole 1245C. Moreover, the PCS data do not constrain the vertical distribution of gas hydrate, and an apparent gradual increase with depth in the gas hydrate

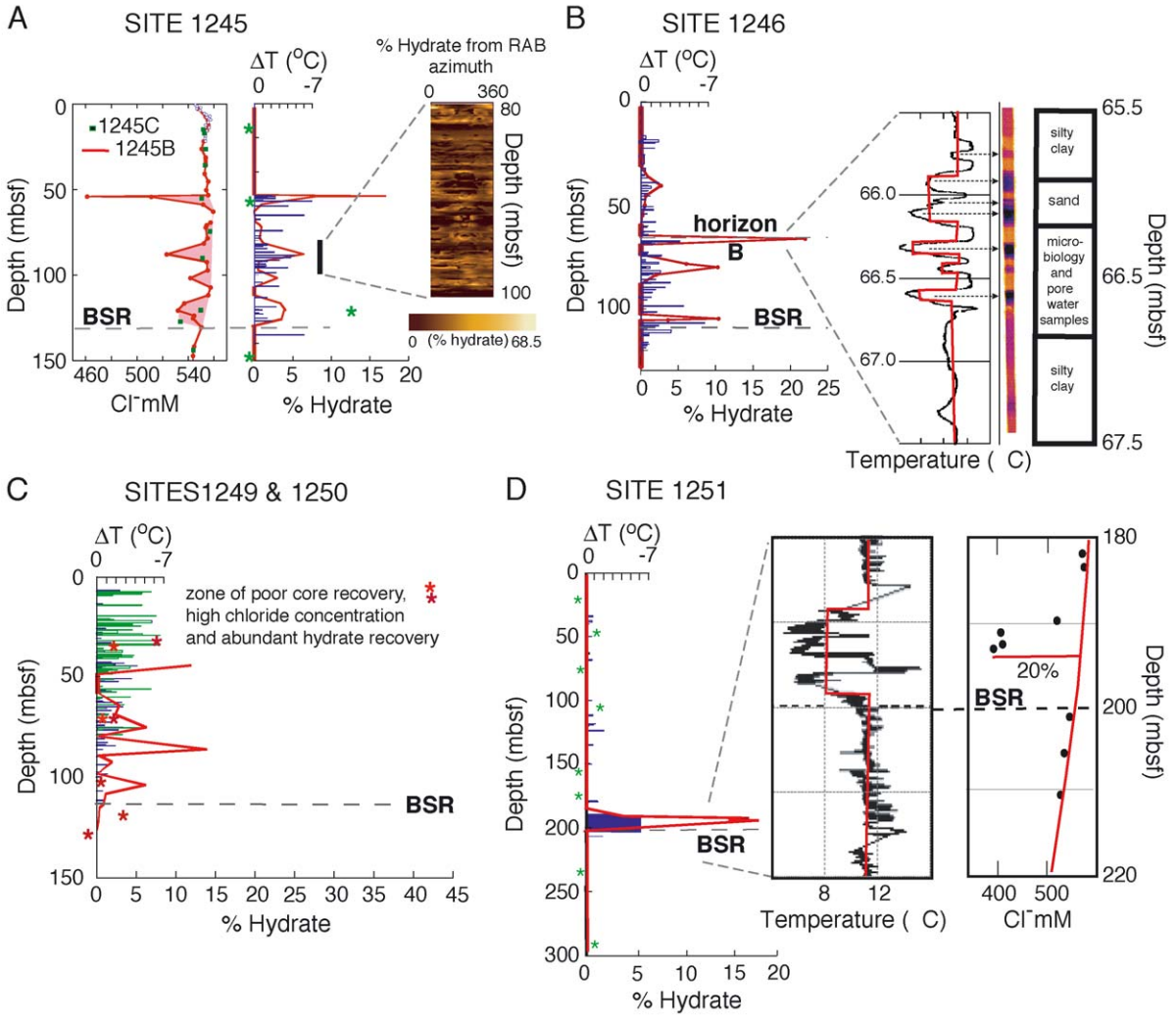

Fig. 6. Comparison of ΔT anomalies (blue or green bars) to gas hydrate content estimated from dilution of Cl^- concentration (red lines) and from degassing of pressure core samplers (green stars, except in Fig. 4C, where stars are red). (A) Site 1245. Expanded section shows lateral variation around the circumference of the borehole from 80 to 100 mbsf estimated from RAB data in Hole 1250B. Resistivity scans were calculated at 56 evenly spaced azimuths around the 10-in. diameter borehole. Gas hydrate content at each position was calculated [31] using average porosity from the LWD density log, grain density and pore water salinity from shipboard measurements, and the geothermal gradient from the in situ temperature tool [20]. Maximum calculated concentration is 83% for a nodule near 93 mbsf. Average concentration in this interval calculated from the RAB data is 8%, similar to that determined from IR and Cl^- data. (B) Site 1246. Expanded section shows the IR temperature anomaly associated with the lower of two coarse-grained layers comprising Horizon B. The picked (ΔT, ΔL) curve (red) is overlain on the temperature profile extracted from the IR images (black). A stratigraphic summary is shown on the right. The onset of the IR anomaly is associated with the top of coarse-grained layer. Unfortunately most of this layer was taken for microbiology samples and its internal structure could not be documented by Leg 204 shipboard sedimentologists. A pore water sample from this zone indicated that hydrate occupied 22% of the pore space. Integration of (ΔT, ΔL) over this zone indicates 28% gas hydrate. (C) Sites 1249 and 1250. (D) Site 1251. Expanded section shows details of the IR thermal anomaly and closely spaced Cl^- concentration measurements from Hole 1251D immediately above the BSR.

content within the GHSZ that is suggested by combining all data from the flanks of Hydrate Ridge [2] may be misleading.

Applying similar reasoning to the Cl^- concentration data and assuming that each pore water sample was derived from 10 cm of core and that a sample must be taken within 5 cm of a hydrate lens for pore waters to be diluted because of hydrate dissociation during recovery, we would expect that only 10% of the samples would "capture" a hydrate lens. However, 33% of the pore water samples suggest >1% hydrate concentration. This probably results: (1) because of a bias towards taking samples for pore water analysis near IR temperature anomalies, which leads to an overestimate of average gas hydrate content, and (2) because small concentrations of disseminated hydrate detected with the chloride concentration data may not have generated significant temperature anomalies, leading to an underestimate. Similarity between average gas hydrate contents calculated from ΔT and Cl^- anomaly data (Table 1) may reflect the combined effect of these two factors.

Good correlation between the envelope of ΔT anomalies and the 27 Cl^- concentration measurements in the GHOZ in Hole 1245B suggests that the number of Cl^- concentration measurements was adequate to resolve the large scale pattern of clustering of hydrate lenses, whereas the sparser spacing of Cl^- measurements in Hole 1245C was inadequate. Error bounds on the amplitude of the concentration versus depth curve obtained from Cl^- concentration data, however, are probably quite large. The sample from Hole 1245B at 53 mbsf, which yields a concentration estimate of 17% of pore volume, may have fortuitously captured a 1-cm-thick hydrate lens within the 10-cm-long sample taken for this analysis. Other samples suggest much lower concentrations.

Because little or no hydrate is indicated in Cl^- concentration or PCS data at a similar depth in Hole 1245C, located 50 m from Hole 1245B, we infer that hydrate lenses are discontinuous at this scale. This is consistent with large variations between holes at Sites 1244, 1246, and 1251 based on the IR and RAB data. We interpret the variations to indicate patchy clusters of high gas hydrate concentration.

6. Regional variations in gas hydrate distribution

Results in Table 1 have been grouped according to the end-member structural settings discussed in Section 2. Average gas hydrate content in each setting is summarized in Table 2.

6.1. Southern Hydrate Ridge flanks

Based on the data in these tables, we further divide the region of Hydrate Ridge away from the summit into two subregions: the western flank, which is characterized by folded sediments in which faulting is rare (1245 and 1247), and the eastern flank, which is characterized by pervasive faulting (Sites 1244 and 1246). The data for holes at Sites1245 and 1247 are remarkably consistent. The mean gas hydrate content of the GHSZ is 1.7±0.2% (Table 2). Averaged over the GHOZ, the mean is 2.7±0.8%.

Sites 1244 and 1246 show greater variability, with two out of five holes indicating gas hydrate content

Table 2
Mean and standard deviation of gas hydrate content in the pore space in regions with different seismic reflection characteristics

Sites	Hole 1	Hole 2	Hole 3	Hole 4	Hole 5	Mean and standard deviation
1245 and 1247	1245A	1245B	1245C	1247A	1247B	
GHSZ	1.9	1.9	1.6	1.6	1.7	1.74±0.15
GHOZ	3.1	3.8	2.9	2.0	1.9	2.74±0.80
1244 and 1246	1244B	1244C	1244E	1246A	1246B	
GHSZ	6.1	2.0	2.1	1.0	5.0	3.24±2.19
GHOZ	8.1	3.2	2.6	1.5	5.6	4.20±2.65
1251 and 1252	1251A	1251B	1251D	1252A		
GHSZ	1.0	1.2	4.5	1.3		2.00±1.67
GHOZ	1.2	1.6	5.2	1.9		2.48±1.84

The average for each hole was taken from Table 1. Only IR and RAB data are included because those estimates are based on hundreds of data points that sample most of the GHSZ. Inclusion of estimates from Cl^- and PCS data, weighted by the fraction of the GHSZ sampled by those measurements (<3% in for all holes), would not affect these estimates. Data for the summit region were not included in this table because of the large uncertainty in the IR data due to poor recovery and the probable errors due to the presence of free gas in RAB-based estimates at Site 1249.

>5% averaged over the GHSZ (Table 1). In Hole 1246B, this is due to an apparently high concentration of gas hydrate associated with seismic Horizon B, which results from two coarse-grained layers located ~9 m apart that preferentially contain gas hydrate based on IR and Cl^- concentration anomalies (Fig. 6B, insert). This layer is not, however, detected in RAB data from Hole 1246A. On the other hand, RAB data from Hole 1244B indicates high concentrations of gas hydrate distributed in steeply dipping fractures (see Fig. F8 in the Leg 204 Preliminary Report [14]), but no anomalously high amount of gas hydrate was detected with Cl^- concentrations or in the IR data in Hole 1244C. We attribute the greater variability among boreholes at these two sites to pervasive small-offset faults (Fig. 2A) that permit more vigorous upward fluid flow and concentration of gas hydrate in patches along faults and in favorable lithologies. We then use the seismic data to map a region in which discontinuous patches of relatively high gas hydrate content increase the average gas hydrate content to 3.2±2.2% in the GHSZ (Fig. 1B) or 4.2±2.7% in the GHOZ (Fig. 2A).

6.2. Southern Hydrate Ridge summit

Beneath the summit (Figs. 2B and 6C), where persistent, vigorous venting of methane bubbles at the seafloor has been documented [35], all data indicate very high concentrations of gas hydrate in the upper 20–40 m [20,28,29]. Cores contained hydrate in massive chunks, lenses, nodules, and thin plates. At Site 1249, the ΔT anomalies in this depth range are strong and closely spaced, with gaps due primarily to poor recovery, and indicate hydrate content of ~25%. ODP and HYACINTH pressure cores recovered from Site 1249 at 8 and 14 mbsf, respectively, indicate hydrate content of ~45% [2,20]. Cl^- concentration and RAB data also indicate abundant gas hydrate at this site, although hydrate content cannot be quantified from these data because underlying assumptions for these two methods are violated (see Sections 3.1 and 3.2). Considering that the ΔT-based estimates are probably underestimated because of poor recovery, and that pressure core samples may be overestimated because their locations were chosen based on evidence in the RAB data for layers of high hydrate concentration [20], we suggest that 30–40% is a reasonable estimate for the average gas hydrate content in the upper 20–40 mbsf at these sites. Below ~30 mbsf, recovery improved considerably. Cl^- concentration, ΔT anomalies, and PCS data suggest that hydrate distribution and concentration at these depths is similar to, or only slightly higher than, that beneath the flanks of southern Hydrate Ridge. Similar results are obtained at Sites 1248 and 1250, although the near-surface zone of high hydrate content at Site 1250 is thinner (~15 m).

The base of the region of very high hydrate content at the summit is correlated with the base of a zone of near-surface, high-amplitude, chaotic seismic reflections at Sites 1249 and 1250, and the lateral extent of this seismic pattern is coincident with moderate-to-high seafloor acoustic backscatter (Fig. 7). We estimate the size of this concentrated gas hydrate deposit to be approximately 300 by 500 by 30 m; the amount of methane trapped in this deposit is therefore 1.5–2×10^8 m^3 at STP. If the region beneath the carbonate pinnacle, which was not sampled by drilling, is excluded from this estimate, the total amount of gas is decreased by ~20%. This association of high gas hydrate content with distinctive patterns of seafloor and subsurface reflectivity may permit mapping concentrated near-surface gas hydrate deposits elsewhere.

6.3. Eastern slope basin

Beneath the slope basin east of southern Hydrate Ridge (Site 1251), the distribution and concentration of gas hydrate is different from the two flank and summit environments discussed above. ΔT anomalies are, on average, widely spaced and of low amplitude (Figs. 2C and 4D). Three out of six PCS cores show methane concentration slightly above saturation [2,20], indicating ~1% hydrate in the pore space, similar to the concentration of 1.0% indicated by RAB data in Hole 1251A and 1.2% indicated by ΔT anomalies in Hole 1251B. Although chloride concentration decreased smoothly, presumably because of equilibration with low chloride fluid from deep in the accretionary complex, no anomalous local dilution of chloride concentration was observed [20]. We conclude that the average hydrate content of the slope basin is very low. This may be due in part to very rapid recent deposition of turbidites and debris flows that consist of reworked sediments low in metabolizable organic matter.

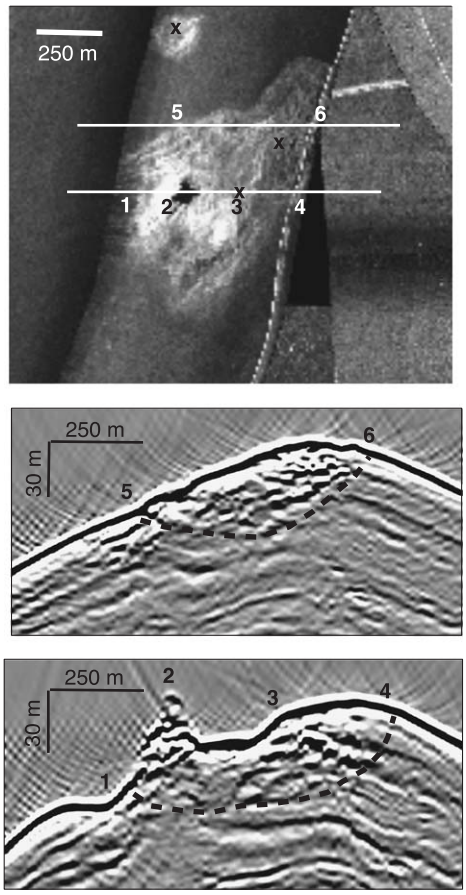

Fig. 7. Correlation between seafloor and subsurface reflectivity near the summit. Upper panel shows seafloor reflectivity from deep-towed sidescan sonar data [17]. Lines indicate location of two seismic sections extracted from the 3D seismic reflection volume. "x" shows the locations of ODP sites. See Fig. 1B for site labels. Numbers on the sidescan sonar and seismic images indicate collocated points. The highest seafloor reflectivity is associated with the carbonate pinnacle. Mottled reflectivity, both on the seafloor and in the subsurface, is associated with the presence of massive hydrate.

An exception to the observation of low hydrate concentration in the basin occurs in a 12-m-thick zone immediately above the BSR in Hole 1251D, which is characterized by an exceptionally strong and persistent IR anomaly (Fig. 4D). Cl^- concentration anomalies from several samples in this zone suggest that the hydrate content is ~20% (Fig. 6D, insert). Small white grains in the pore space were reported, based on visual inspection of the core immediately after recovery, but were not present when samples preserved in liquid nitrogen were examined later, perhaps because gas hydrate dissociated before the cores cooled to ~−60 °C (the temperature for hydrate stability at 1 atm). No pressure cores were obtained from this interval for comparison. We note that in Hole 1251B, we were not able to recover any sediment from this zone using the advanced piston core (APC). Based on the observation that coring with the extended core barrel (XCB) resulted in colder cores (Fig. 4B), we used the XCB on our second attempt to core this zone and were successful. This layer does not appear in the RAB data from Hole 1251A, located ~50 m away, suggesting a patchy distribution.

Inclusion of this basal hydrate-rich layer increases the estimate of the average gas hydrate content of the slope basin by a factor of 2. This may be an underestimate if the layer was present but not sampled in Hole 1251B. This lens of high gas hydrate concentration is probably related to free gas in dipping stratigraphic horizons, as indicated by the strong amplitude of dipping reflections beneath the BSR (Fig. 2C). Based on the seismic data, which indicate that the high amplitude reflectivity does not extend everywhere beneath the basin, the lateral extent of this layer is shown in Fig. 1B. We note that this deep layer of high hydrate content is along strike with an enigmatic alignment of vents along the boundary between Hydrate Ridge and the slope basin to the east [16,17] and speculate that these vents formed in response to uplift and destabilization of similar gas hydrate-rich lenses near the base of the gas hydrate stability zone.

Although a few low-amplitude IR temperature anomalies were reported from Site 1252, no PCS or RAB data were obtained and no chloride concentration anomalies were observed. If gas hydrate is present at this site, it must be in very low concentration. We note that this site is adjacent to a buried anticlinal structure that contains a strong BSR. Based on multiple small faults in strata at the crest of the anticline and other characteristics of the seismic data, we speculate that gas hydrate is present in this structure.

7. Comparison to other areas

Our estimates of the gas hydrate content of the accretionary complex everywhere but near the sea-

floor at the summit of the structure are similar to the average concentration of 2–7% estimated for sediments of the Blake Ridge [36,37], although the total amount of methane per unit area beneath Blake Ridge is greater because of the greater thickness of the GHSZ and greater methane solubility beneath Blake Ridge. Our estimates are significantly lower than estimates of 20–35% that have been reported for the northern Cascadia margin offshore Vancouver [27], which is in a structurally and stratigraphically similar setting. The northern Cascadia estimates are based primarily on geophysical and Cl^- anomaly data from ODP Site 889 and depend strongly on assumed baselines [27]. Our results suggest that these estimates should be reevaluated.

8. Implications and consequences of heterogenous gas hydrate distribution

Through integration of a variety of methods with different spatial resolution and sensitivity to gas hydrate content, we have obtained the first high-resolution estimate of the three-dimensional distribution of gas hydrate within an accretionary ridge system. Spatial variability in gas hydrate distribution determined from ODP drilling data has been correlated with stratigraphic and structural patterns imaged in high-resolution 3D seismic data and provides new insights into the possible response of marine gas hydrates to tectonic and environmental change. The small amount of gas hydrate present, when averaged over the entire study region, supports conservative estimates of the global volume of methane stored in gas hydrate. This leads to questions about whether the role of gas hydrates in driving global change [2] or as a global fossil fuel resource [4] is as important as has been hypothesized [1]. High concentrations of gas hydrate, however, are present locally and may be of commercial value in the future [5]. Deposits of massive hydrate found near the seafloor should respond rapidly to regional or global ocean warming or changes in sea level, as has been hypothesized in global climate change scenarios, if they are located on the continental slope near the upper limit of the hydrate stability zone. These deposits are also susceptible to disruption by earthquakes, during which large, buoyant blocks of gas hydrate may be detached from the seafloor; these blocks will rapidly float to the sea surface, where they will dissociate and vent methane directly to the atmosphere [18]. Relatively high concentrations of gas hydrate are also found at depth in patchy zones several meters thick. These zones may be destabilized by tectonic uplift, producing inversions in sediment strength and fluid/gas pressure that may drive venting and slope instability. This phenomenon may be responsible for an enigmatic alignment of vent-like structures observed along the eastern flank of Hydrate Ridge north of Site 1251 [16,17].

The results of this study also provide a challenge for models of gas hydrate formation in nature and for models to derive gas hydrate content from seismic and other remote sensing data. Although the observations are consistent with microscopic scale models that predict differences in hydrate distribution as a function of sediment grain size [38], the heterogeneity at larger scales is not explained by currently available quantitative models for the vertical distribution of gas hydrate within the hydrate stability zone [39–41], which all predict gradual changes in gas hydrate concentration with depth. Time-dependent models that include multiphase fluid flow in a heterogeneous medium are needed.

Acknowledgements

This project was supported by the Ocean Drilling Program, funded by the U.S. National Science Foundation and other international partners. We thank the Master and crew of the JOIDES Resolution for making this cruise a success. The ODP technical staff showed remarkable flexibility and good humor in addressing the numerous exceptional challenges posed by drilling for gas hydrate. The RAB image in Fig. 6A was constructed by A. Janik. Martin Hovland and Bill Dillon provided helpful reviews. ***[BOYLE]***

References

[1] K.A. Kvenvolden, T.D. Lorenson, The global occurrence of natural gas hydrate, in: C.K. Paull, W.P. Dillon (Eds.), Natural Gas Hydrates: Occurrence, Distribution and Detection, Geophysical Monograph, vol. 124, American Geophysical Union, 2001, pp. 3–18.

[2] A.V. Milkov, G.E. Claypool, Y.-J. Lee, W. Xu, G.R. Dickens, W.S. Borowski, ODP Leg 204 Scientific Party, In situ methane concentrations at Hydrate Ridge, offshore Oregon: new constraints on the global gas hydrate inventory from an active margin, Geology 31 (2003) 833–836.
[3] G.R. Dickens, Rethinking the global carbon cycle with a large, dynamic and microbially mediated gas hydrate capacitor, Earth Planet. Sci. Lett. 213 (2003) 169–183.
[4] M. Hovland, Are there commercial deposits of methane hydrates in ocean sediments? Energy Explor. Exploit. 18 (2000) 339–347.
[5] A.V. Milkov, R. Sassen, Economic geology of offshore gas hydrate accumulations and provinces, Mar. Pet. Geol. 19 (2002) 1–11.
[6] G.R. Dickens, M.M. Castillo, J.C.G. Walker, A blast of gas in the latest Paleocene, Geology 25 (1997) 259–262.
[7] M.E. Katz, D.K. Pak, G.R. Dickens, K.G. Miller, The source and fate of massive carbon input during the Latest Paleocene Thermal Maximum, Science 286 (1999) 1531–1533.
[8] J.P. Kennett, K.G. Cannariato, I.L. Hendy, R.J. Behl, Methane hydrates in quaternary climate change: the clathrate gun hypothesis, Am. Geophys. Un. Spec. Publ. S4 (2003) (216 pp.).
[9] S. Chand, T.A. Minshull, Seismic constraints on the effects of gas hydrate on sediment physical properties and fluid flow: a review, Geofluids 3 (2003) 275–289.
[10] K.M. Brown, N.L. Bangs, P.N. Froelich, K.A. Kvenvolden, The nature, distribution, and origin of gas hydrate in the Chile Triple Junction region, Earth Planet. Sci. Lett. 139 (1996) 471–483.
[11] M. Kastner, K.A. Kvenvolden, M.J. Whiticar, A. Camerlenghi, T.D. Lorenson, Relation between pore fluid chemistry and gas hydrates associated with bottom-simulating reflectors at the Cascadia margin, Sites 889 and 892, in: B. Carson, G.K. Westbrook, R.J. Musgrave, E. Suess (Eds.), Proc. ODP, Sci. Results 146 (Pt. 1), Ocean Drilling Program, College Station TX, 1995, pp. 375–384.
[12] C.K. Paull, R. Matsumoto, Leg 164 overview, in: C.K. Paull, R. Matsumoto, P.J. Wallace, W.P. Dillon (Eds.), Proc. ODP, Sci. Results 164, Ocean Drilling Program, College Station TX, 2000, pp. 3–10.
[13] M.J. Whiticar, M. Hovland, M. Kaster, J.C. Sample, Organic geochemistry of gases, fluids, and hydrates at the Cascadia accretionary margin, in: B. Carson, G.K. Westbrook, R.J. Musgrave, E. Suess (Eds.), Proc. ODP, Sci. Results 146 (Pt. 1), Ocean Drilling Program, College Station TX, 1995, pp. 385–398.
[14] M. Hovland, D. Lysne, M. Whiticar, Gas hydrate and sediment gas composition, Hole 892A, in: B. Carson, G.K. Westbrook, R.J. Musgrave, E. Suess (Eds.), Proc. ODP, Sci. Results 146 (Pt. 1), Ocean Drilling Program, College Station TX, 1995, pp. 151–162.
[15] M.E. MacKay, R.D. Jarrad, G.K. Westbrook, R.D. Hyndman, Leg 146 Shipboard Scientific Party, Origin of bottom simulating reflectors: geophysical evidence from the Cascadia accretionary complex, Geology 22 (1994) 459–462.
[16] A.M. Tréhu, M.E. Torres, E. Suess, G. Bohrmann, G. Moore, Temporal and spatial evolution of a gas-hydrate-bearing ridge on the Oregon continental margin, Geology 27 (1999) 939–942.
[17] J.E. Johnson, C. Goldfinger, E. Suess, Geophysical constraints on the surface distribution of authigenic carbonates across the Hydrate Ridge region, Mar. Geol. 202 (2003) 79–120.
[18] E. Suess, et al., Seafloor methane hydrates at Hydrate Ridge, Cascadia margin, in: C.K. Paull, W.P. Dillon (Eds.), Natural Gas Hydrates: Occurrence, Distribution and Detection, Geophysical Monograph, vol. 124, American Geophysical Union, 2001, pp. 87–98.
[19] M.E. Torres, J. McManus, D.E. Hammond, M.A. de Angelis, K.U. Heeschen, S.L. Colbert, M.D. Tryon, K.M. Brown, E. Suess, Fluid and chemical fluxes in and out of sediments hosting methane hydrate deposits on Hydrate Ridge, OR: Part 1. Hydrologic provinces, Earth Planet. Sci. Let. 201 (2002) 525–540.
[20] A.M. Tréhu, G. Bohrmann, F. Rack, M.E. Torres, Leg 204 Scientific Party, Proc. ODP, Initial Reports, 204 [CD-ROM]. Available from: Ocean Drilling Program, Texas A&M University, College Station TX 77845-9547, 2003.
[21] A.M. Tréhu, P.B. Flemings, P.B. Leg 204 Scientific Party, Lithostatic gas pressures and venting at southern Hydrate Ridge (abs.), Fall Meet. Suppl., Eos. Trans. AGU, vol. 84 (46), 2003, OS51C-0871.
[22] T.L. Pettigrew, The design and operation of a wireline pressure core sampler (PCS), ODP Tech. Note 17 (1992).
[23] G.R. Dickens, P.J. Wallace, C.K. Paull, W.S. Borowski, Detection of methane gas hydrate in the pressure core sampler (PCS): volume–pressure–time relations during controlled degassing experiments, in: C.K. Paull, R. Matsumoto, P.J. Wallace, W.P. Dillon (Eds.), Proc. ODP, Sci. Results, vol. 164, Ocean Drilling Program, College Station, TX, 2000, pp. 113–126.
[24] R. Hesse, W.E. Harrison, Gas hydrates causing pore-water freshening and oxygen isotope fractionation in deep-water sedimentary section of terrigenous continental margins, Earth Planet. Sci. Lett. 55 (1981) 453–462.
[25] P.K. Egeberg, G.R. Dickens, Thermodynamic and pore water halogen constraints on gas hydrate distribution at ODP Site 997 (Blake Ridge), Chem. Geol. 153 (1999) 53–79.
[26] W. Ussler III, C.K. Paull, Ion exclusion associated with marine gas hydrate deposits, in: C.K. Paull, W.P. Dillon (Eds.), Natural Gas Hydrates: Occurrence, Distribution and Detection, Geophysical Monograph, vol. 124, American Geophysical Union, 2001, pp. 41–52.
[27] R.D. Hyndman, G.D. Spence, R. Chapman, M. Reidel, R.N. Edwards, Geophysical studies of marine gas hydrate in northern Cascadia, in: C.K. Paull, W.P. Dillon (Eds.), Natural Gas Hydrates: Occurrence, Distribution and Detection, Geophysical Monograph, vol. 124, American Geophysical Union, 2001, pp. 273–295.
[28] M.E. Torres, K. Wallman, A.M. Tréhu, G. Bohrmann, W.S. Borowski, H. Tomaru, Gas hydrate dynamics at the southern summit of Hydrate Ridge, Cascadia margin, Earth Plan. Sci. Lett. (in review).
[29] A. Milkov, G.R. Dickens, G.E. Claypool, Y.-J. Lee, W.S. Borowski, M.E. Torres, W. Xu, H. Tomaru, A.M. Tréhu, P. Schultheiss, Co-existence of gas hydrate free gas, and brine

within the regional gas hydrate stability zone at the southern summit of Hydrate Ridge (Oregon margin): evidence from prolonged degassing of a pressurized core, Earth Planet. Sci. Lett. 222 (2004) 829–843. doi:10.1016/j.epsl.2004.03.028.

[30] K.H. Ford, T.H. Naehr, C.G. Skilbeck, C.G. Leg 201 Scientific Party, The use of infrared thermal imaging to identify gas hydrate in sediment cores, in: S.L. D'Hondt, B.B. Miller, D.J. Miller, et al. (Eds.), Proc. ODP, Initial Reports, vol. 201, Ocean Drilling Program, College Station, TX, 2003, pp. 1–20.

[31] T.S Collett, J. Ladd, Detection of gas hydrates with downhole logs, in: C.K. Paull, R. Matsumoto, P.J. Wallace, W.P. Dillon (Eds.), Proc. ODP, Sci. Results, vol. 164, Ocean Drilling Program, College Station TX, 2000, pp. 179–191.

[32] T.S. Collett, D.S. Goldberg, A. Janik, G. Guerin, G. Leg 204 Scientific Party, Downhole log assessment of gas hydrate and free gas concentrations on Hydrate Ridge (abs.), Fall Meet. Suppl., Eos. Trans. AGU, vol. 84 (46), 2003, OS51C-0876.

[33] G. Guerin, D. Goldberg, A. Melster, Characterization of in situ elastic properties of gas hydrate-bearing sediments on the Blake Ridge, J. Geophys. Res. 104 (1999) 17781–17795.

[34] N.L. Bangs, I. Pecher, A.M. Tréhu, A.M. Leg 204 Scientific Party, Lithostatic gas pressures and venting at southern Hydrate Ridge (abs.), Fall Meet. Suppl., Eos. Trans. AGU, vol. 84 (46), 2003, OS52C-01.

[35] K.U. Heeschen, A.M. Tréhu, R.W. Collier, E. Suess, G. Rehder, Distribution and height of methane bubble plumes on the Cascadia margin characterized by acoustic imaging, Geophys. Res. Let. 30 (2003) 1643–1646.

[36] G.R. Dickens, et al., Direct measurement of in situ methane quantities in a large gas-hydrate reservoir, Nature 385 (1997) 426–428.

[37] W.S. Holbrook, et al., Methane hydrate and free gas on the Blake Ridge from vertical seismic profiling, Science 273 (1996) 1840–1843.

[38] B. Clennell, M. Hovland, J.S. Booth, P. Henry, W.J. Winters, Formation of natural gas hydrates in marine sediments: 1. Conceptual model of gas hydrate growth conditioned by host sediment properties, J. Geophys. Res. 104 (1999) 22003–22985.

[39] X.-Y Xu, C. Ruppel, Predicting the occurrence, distribution and evolution of methane gas hydrate in porous marine sediments, J. Geophys. Res. 104 (1999) 5081–5095.

[40] M.K. Davie, B.A. Buffet, A numerical model for the formation of gas hydrate below the seafloor, J. Geophys. Res. 106 (2001) 497–514.

[41] D.F. Chen, L. Cathles III, A kinetic model for the pattern and amounts of hydrate precipitated from a gas stream, J. Geophys. Res. 108 (2003) 2058–2071.

[42] D. Clague, N. Maher, C.K. Paull, High-resolution multibeam survey of Hydrate Ridge, offshore Oregon, in: C.K. Paull, W.P. Dillon (Eds.), Natural Gas Hydrates: Occurrence, Distribution and Detection, Am. Geophys. Union Geophys. Monogr. 124 (2001) 297–306.